Numerical Solutions of Scramjet Nozzle Flows

J. A. Schetz,* F. S. Billig,† and S. Favin‡
The Johns Hopkins University Applied Physics Laboratory, Laurel, Maryland

The accurate prediction of nozzle flows for ramjets and scramjets is important for design and system performance analysis. The problem is made complex by the presence of strongly nonuniform entrance profiles, especially for scramjets (which have no throat at the end of the combustor). Thus, turbulent mixing and, often, chemical reactions can be expected to be under way during the expansion process. The rapid expansion common in nozzles implies substantial radial pressure gradients. Taken together, these requirements lead to the necessity of utilizing the full Navier-Stokes equations for a compressible, multicomponent, turbulent flow with finite-rate chemistry. For this work, the unsplit, explicit, MacCormack unsteady/finite-difference method was used to solve the equations of motion. Turbulence transport is represented with a turbulent kinetic energy model. Chemistry is treated at this time by either frozen equilibrium or a simple, global finite-rate model. Calculations are presented for a typical scramjet case where the effects of nonuniform inflow profiles on the nozzle flowfield and performance are shown for different nozzle designs.

Nomenclature

a = speed of sound
b = mixing zone width
C_i = species mass fraction
c_p = specific heat at constant pressure
c_v = specific heat at constant volume
C_{ML}, C_q, C_μ = constants in turbulence models
$D( )/Dt$ = substantial derivative
D_{ij} = binary diffusion coefficient
D_T = binary eddy diffusion coefficient
e = internal energy
e_i^0 = energy of formation of specie i
h = enthalpy
h_i^0 = heat of formation of specie i
k = molecular thermal conductivity
k_T = eddy thermal conductivity
ℓ_m = mixing length
M = Mach number
p = pressure
Pr_T = turbulent Prandtl number
$\bar{q}$ = total heat flux vector
q = turbulent kinetic energy
$\Re$ = universal gas constant
Sc_T = turbulent Schmidt number
t = time
u = streamwise velocity
v = transverse (radial) velocity
$\bar{V}$ = velocity vector
$\dot{w}_i$ = chemical production rate
W = mixture molecular weight
W_i = specie molecular weight
x = streamwise coordinate
y = transverse (radial) coordinate
ρ = mixture density
μ = molecular viscosity and total viscosity
μ_T = eddy viscosity
λ = second molecular viscosity coefficient and total second viscosity
λ_T = second eddy viscosity coefficient, $= \lambda\mu_T/\mu$
γ = ratio of specific heats
ϵ = 0 for planar flow, 1 for axisymmetric flow
Φ = viscous dissipation
$\bar{\bar{\tau}}$ = viscous stress tensor

Presented as Paper 85-1270 at the AIAA/SAE/ASME/ASEE 21st Joint Propulsion Conference, Monterey, CA, July 8-10, 1985; received Oct. 26, 1985; revision received March 10, 1986.

*Consultant; also Professor and Head, Aerospace and Ocean Engineering Department, Virginia Polytechnic Institute and State University, Blacksburg. Fellow AIAA.
†Assistant Supervisor, Aeronautics Department. Fellow AIAA.
‡Senior Programmer.

Introduction

ALL aerospace propulsion systems require the design of efficient components in order to achieve good system performance. For ramjet systems, especially those for high Mach number flight utilizing supersonic combustion (scramjets), the requirements on component performance are particularly severe (cf, Ref. 1). Furthermore, the distinction between the airframe and the engines or, indeed, between the engine components themselves become less and less clear for high Mach number vehicles. The fuselage and the inlet are merged and, for scramjets, the combustor and the nozzle can be viewed as two parts of the same "component."

Some area increase in the "combustor" is usually required to prevent thermal choking, but the rate of area increase must not be so large as to lead to extinguishing the flame. In as short a distance as possible after the heat release is complete, it is desirable to begin the "nozzle" expansion process. This is desirable to minimize overall system length and to limit the surface area of high pressure and thus high skin friction. In scramjets, overall system performance is very sensitive to internal skin friction.[1] Starting the expansion process soon after the end of heat release means very nonuniform profiles of temperature and concentration (and thus density and mass flux) entering the "nozzle." Most scramjets are designed to avoid losses and complications due to shocks in the combustor, so transverse static pressure variations are often not large. One other facet of scramjets is very important here. Since the flow in the combustor is supersonic, there is no contraction (acceleration) or throat for the nozzle, as in rockets, ramjets, or jet engines. Thus, the strong lessening of nonuniformities resulting from rapid axial acceleration of the stream is not present in scramjets.

Taken together, these considerations require the accurate design of efficient nozzles with strongly nonuniform, supersonic inflows. It can be expected that turbulent mixing will continue during the expansion process, so a viscous analysis

is necessary. Finally, chemical reaction effects can be important. The recombination of H, O, OH, etc., present in significant amounts at the end of the combustor (and thus the beginning of the nozzle) at some flight conditions in the rapidly falling static temperature and pressure environment of the expansion process can have an important influence on nozzle performance.

The development of an analysis with these capabilities is the subject of this paper. There was relatively little directly relevant prior work on nozzles per se to draw upon (e.g., Refs. 2–10). Earlier work on scramjets has focused much more on inlets and combustors (e.g., Refs. 2–15) than on nozzles. The combustor analyses have generally neglected transverse static pressure gradients (i.e., a boundary-layer equation formulation is used), so they are not easily extended to the nozzle expansion process where such variations are important.

The analysis presented below attempts to include the major processes discussed. It does, however, have some restrictions and limitations that are imposed primarily by computer capacity and cost considerations. The formulation is based on the full, elliptic Navier-Stokes equations. A boundary-layer equation formulation was rejected, since transverse pressure gradients are significant. A parabolized, Navier-Stokes (PNS) formulation was rejected for three reasons: 1) the authors are uneasy about some of the manipulations necessary to make PNS codes perform in some flows; 2) in the long term, treatment of streamwise separation may be desired; and 3) the formulation adopted below is competitive with PNS on a cost basis. The geometry is, at present, restricted to two dimensions—planar or axisymmetric. The formulation is unsteady, but this is for computational convenience. The steady flow is calculated as the end result of a transient flow development. Turbulent transport is modeled with a one-equation, turbulent kinetic energy (TKE) model. The details of the wall boundary layer are calculated separately from the main core flow with a TKE boundary-layer code. This same philosophy was used with good success in the combustor analysis in Ref. 13.

The result of this procedure is a great savings in computer costs because of the different grid resolution requirements in the two regions of the flow. Good turbulent boundary-layer solutions require at least 60–80 points across the thin layer (no matter how they are arranged) to get accurate values for the skin friction and heat transfer. On the other hand, good resolution of the core flow can be obtained with 20–30 points across a much thicker viscous zone. Boundary-layer equations cannot be used in the nozzle core flow because of the large transverse pressure variations. However, one does not want to use the Navier-Stokes equations in the wall boundary layer where the transverse pressure gradients are indeed negligible. The gas composition is limited to molecules formed with H, C, O, and N atoms. The numerical scheme used is the explicit, unsplit MacCormack method,[16] and the implementation follows the perfect gas, single-specie code of Cline.[17]

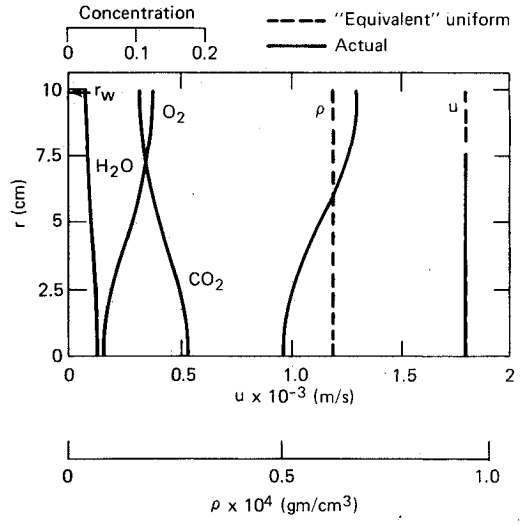

Fig. 1 Inlet profiles used for nozzle flowfield calculations.

Analysis

Equations of Motion

The two-dimensional, Reynolds-averaged Navier-Stokes equations for compressible, turbulent flow may be written as follows.

Global continuity:

$$\frac{\partial \rho}{\partial t}+u\frac{\partial \rho}{\partial x}+v\frac{\partial \rho}{\partial y}+\rho\left(\frac{\partial u}{\partial x}+\frac{\partial v}{\partial y}+\frac{\epsilon v}{y}\right)=0 \tag{1}$$

Streamwise momentum conservation:

$$\frac{\partial u}{\partial t}+u\frac{\partial u}{\partial x}+v\frac{\partial u}{\partial y}+\frac{1}{\rho}\frac{\partial p}{\partial x}$$
$$=\frac{1}{\rho}\frac{\partial}{\partial x}\left[(\lambda+2\mu)\frac{\partial u}{\partial x}+\lambda\frac{\partial v}{\partial y}\right]$$
$$+\frac{1}{\rho}\frac{\partial}{\partial y}\left[\mu\left(\frac{\partial v}{\partial x}+\frac{\partial u}{\partial y}\right)\right]$$
$$+\frac{\epsilon}{\rho y}\left[(\lambda+\mu)\frac{\partial v}{\partial x}+\mu\frac{\partial u}{\partial y}\right]-\frac{1}{\rho}\frac{2}{3}\frac{\partial \rho q}{\partial x} \tag{2}$$

Transverse momentum conservation:

$$\frac{\partial v}{\partial t}+u\frac{\partial v}{\partial x}+v\frac{\partial v}{\partial y}+\frac{1}{\rho}\frac{\partial p}{\partial y}$$
$$=\frac{1}{\rho}\frac{\partial}{\partial y}\left[(\lambda+2\mu)\frac{\partial v}{\partial y}+\lambda\frac{\partial u}{\partial x}\right]$$
$$+\frac{1}{\rho}\frac{\partial}{\partial x}\left[\mu\left(\frac{\partial v}{\partial x}+\frac{\partial u}{\partial y}\right)\right]$$
$$+\frac{\epsilon}{\rho y}\left[(\lambda+2\mu)\left(\frac{\partial v}{\partial y}-\frac{v}{y}\right)\right]-\frac{1}{\rho}\frac{2}{3}\frac{\partial \rho q}{\partial y} \tag{3}$$

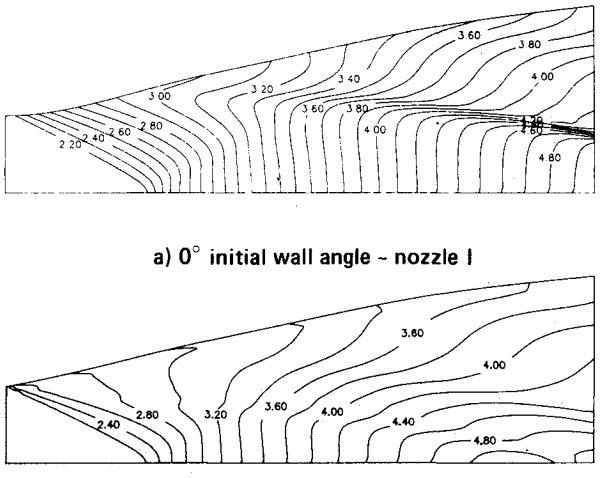

Fig. 2 Design nozzle contours with inviscid Mach number variation for "equivalent" uniform inflow and $\gamma = 1.4$.

These have to be supplemented in this work by equations for species conservation, written here in terms of mass fractions, one for each specie i.

Species continuity:

$$\frac{\partial C_i}{\partial t}+u\frac{\partial C_i}{\partial x}+v\frac{\partial C_i}{\partial y}=\frac{1}{\rho}\frac{\partial}{\partial x}\left[(\rho D_{ij}+\rho D_T)\frac{\partial C_i}{\partial x}\right] \quad (4)$$

$$+\frac{1}{\rho}\frac{\partial}{\partial y}\left[(\rho D_{ij}+\rho D_T)\frac{\partial C_i}{\partial y}\right]$$

$$+\frac{\epsilon}{\rho y}\left[(\rho D_{ij}+\rho D_T)\frac{\partial C_i}{\partial y}\right]+\frac{\dot{w}_i}{\rho}$$

Here, we have assumed binary diffusion and neglected thermal and pressure diffusion. An equation of state is required,

$$p=\rho\frac{\Re}{W}T \quad (5)$$

where

$$W=1/\sum_i C_i/W_i \quad (6)$$

Of course, conservation of energy must be enforced resulting in an energy equation. For variable density flows, this equation is used in more different forms than any of the other equations. The equation must be derived in terms of the internal energy, but it is usually rewritten in terms of the temperature or enthalpy—in either "static" or "stagnation" form. For numerical computations, it has become common (e.g., Ref. 17) to view the energy equation as the equation for the pressure. In the present case, it was necessary to properly include extra terms for energy transfer as a result of mass transfer. The basic energy equation in terms of the internal energy e is[18]

$$\rho\frac{\mathrm{D}}{\mathrm{D}t}\left(e+\frac{1}{2}V^2\right)=-\nabla\cdot\bar{q}-\nabla\cdot(p\bar{V})+\nabla\cdot(\bar{\bar{\tau}}\cdot\bar{V}) \quad (7)$$

This can be manipulated to give

$$\rho\frac{\mathrm{D}e}{\mathrm{D}t}=-\nabla\cdot\bar{q}-p\nabla\cdot\bar{V}+\Phi \quad (8)$$

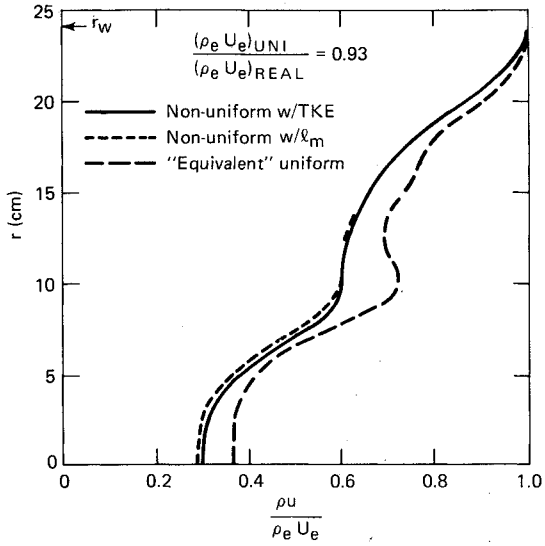

Fig. 3 Nozzle exit Mach number profiles for nozzle I.

Here, $\bar{q}$ is the total heat flux vector and Φ the viscous dissipation. With mass transfer, we have

$$\bar{q}=-(k+k_T)\nabla T-\sum_i h_i(\rho D_{ij}+\rho D_T)\nabla C_i \quad (9)$$

To develop an equation for the pressure, one can begin with the left-hand side of Eq. (8) rewritten using the definition of the internal energy for a mixture of perfect gases

$$\rho\frac{\mathrm{D}e}{\mathrm{D}t}=\rho c_v\frac{\mathrm{D}T}{\mathrm{D}t}+\rho\Sigma e_i\frac{\mathrm{D}C_i}{\mathrm{D}t} \quad (10)$$

Using Eq. (5), this becomes

$$\rho\frac{\mathrm{D}e}{\mathrm{D}t}=\frac{c_v}{\Re}\left[W\frac{\mathrm{D}p}{\mathrm{D}t}-\frac{pW}{\rho}\frac{\mathrm{D}\rho}{\mathrm{D}t}+p\frac{\mathrm{D}W}{\mathrm{D}t}\right]+\rho\Sigma e_i\frac{\mathrm{D}C_i}{\mathrm{D}t} \quad (11)$$

The second term in the brackets can be recast using the continuity equation as

$$-\frac{pW}{\rho}\frac{\mathrm{D}\rho}{\mathrm{D}t}=Wp\nabla\cdot\bar{V} \quad (12)$$

Note that a term like the right-hand side appeared earlier in Eq. (8). Combining, one gets

$$\frac{\mathrm{D}e}{\mathrm{D}t}+p\nabla\cdot\bar{V}=\frac{1}{\gamma-1}\left[\frac{\mathrm{D}p}{\mathrm{D}t}+\frac{p}{W}\frac{\mathrm{D}W}{\mathrm{D}t}-a^2\frac{\mathrm{D}\rho}{\mathrm{D}t}\right]$$

$$+\rho\Sigma e_i\frac{\mathrm{D}C_i}{\mathrm{D}t} \quad (13)$$

where

$$a^2\equiv\gamma p/\rho \quad (14)$$

and

$$c_p-c_v=\Re/W \quad (15)$$

have been used. Finally, the conservation of energy is

$$\frac{\mathrm{D}p}{\mathrm{D}t}+\frac{p}{W}\frac{\mathrm{D}W}{\mathrm{D}t}-a^2\frac{\mathrm{D}\rho}{\mathrm{D}t}=(\gamma-1)\left[\nabla\cdot((k+k_T)\nabla T)\right.$$

$$\left.+\Phi-\rho\Sigma e_i\frac{\mathrm{D}C_i}{\mathrm{D}t}+\nabla\cdot\left(\Sigma h_i(\rho D_{ij}+\rho D_T)\nabla C_i\right)\right] \quad (16)$$

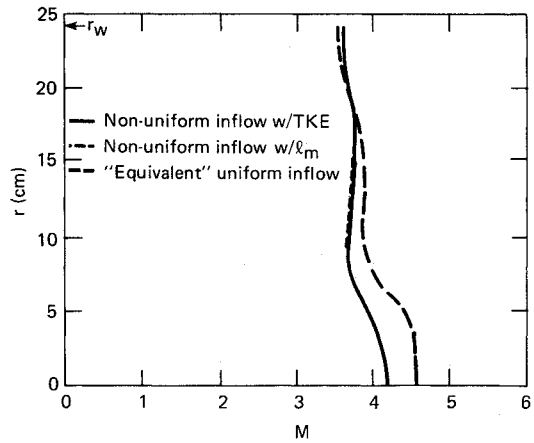

Fig. 4 Nozzle exit mass flux profiles for nozzle I.

which is the form of the energy equation used here to determine the pressure p.

Transport Modeling

In a general treatment, one must calculate the laminar thermophysical properties of the mixture (μ, k, D_{ij}) at all grid points. In reality, that is necessary only in the wall boundary layer out to the logarithmic region. Suitable procedures are described in our earlier work for the combustor wall boundary layer.[13] For the main core flow in the nozzle, we neglect the laminar transport coefficients with respect to the corresponding turbulent coefficients.

The selection of a suitable turbulent transport model always depends upon the problem under study and the goals of the analysis being developed.[19] The flow in the nozzle away from the walls resembles a wake, so a simple algebraic mixing length model might appear appropriate.[19] For the system here, we use

$$\mu_T=\rho\ell_m^2\left[\left(\frac{\partial v}{\partial x}\right)^2+\left(\frac{\partial u}{\partial y}\right)^2\right]^{1/2} \tag{17}$$

$$\ell_m=C_{ML}\cdot b \tag{18}$$

and

$$k_T=c_p\mu_T/Pr_T \tag{19}$$

$$\rho D_T=\mu_T/Sc_T \tag{20}$$

where Pr_T and Sc_T are turbulent Prandtl and Schmidt numbers, both taken here as 0.75, and b is the width of the mixing zone. The proportionality constant C_{ML} is 0.125 for planar flows and 0.11 for axisymmetric flows.

The mixing length model is capable of good predictions of mixing in flows of this type[20] and is simple to implement. However, there are other considerations that can be important here. It can be anticipated that the impingement of the hot combustion products from the nozzle core region on the outer edge of the nozzle wall boundary layer will significantly influence wall heat transfer and skin friction. In addition, the turbulence produced in that mixing zone will also impinge on the wall boundary layer, which can also influence the boundary layer. The effect will be similar to that for a boundary layer with high freestream turbulence. Therefore, we require a prediction of the turbulence level at the outer edge of the viscous core to be used as outer boundary conditions for the wall boundary-layer computation. Thus, we have included the solution of a partial differential equation for the detailed distribution of the TKE. The modeling follows the Prandtl energy method as suggested by Daly and given in Ref. 17. The final form of the TKE equation used here is

$$\begin{aligned}
&\frac{\partial q}{\partial t}+u\frac{\partial q}{\partial x}+v\frac{\partial q}{\partial y}=\frac{2}{3}\frac{q}{\rho}\left(\frac{\partial\rho}{\partial t}+u\frac{\partial\rho}{\partial x}+v\frac{\partial\rho}{\partial y}\right)\\
&+\frac{\lambda_T+2\mu_T}{\rho}\left[\left(\frac{\partial u}{\partial x}\right)^2+\left(\frac{\partial v}{\partial y}\right)\right]^2+\frac{\mu_T}{\rho}\left[\left(\frac{\partial v}{\partial x}\right)^2\right.\\
&\left.+\left(\frac{\partial u}{\partial y}\right)^2\right]+\frac{2\lambda_T}{\rho}\frac{\partial u}{\partial x}\frac{\partial v}{\partial y}+\frac{2\mu_T}{\rho}\frac{\partial v}{\partial x}\frac{\partial u}{\partial y}\\
&+\frac{1}{\rho}\frac{\partial}{\partial x}\left[(\mu+\mu_T)\frac{\partial q}{\partial x}\right]+\frac{1}{\rho}\frac{\partial}{\partial y}\left[(\mu+\mu_T)\frac{\partial q}{\partial y}\right]\\
&-\frac{2\sqrt{2}q^{3/2}}{C_q\ell_m}+\frac{\epsilon}{y}\left[\frac{\lambda_T+2\mu_T}{\rho}\frac{v^2}{y}\right.\\
&\left.+\frac{2\lambda_T v}{\rho}\left(\frac{\partial u}{\partial x}+\frac{\partial v}{\partial y}\right)+\frac{\mu}{\rho}\frac{\partial q}{\partial y}\right]
\end{aligned} \tag{21}$$

where $C_q=17.2$ for planar flows and 12.3 for asixymmetric flows. The eddy viscosity is determined from q with

$$\mu_T=0.3534C_\mu C_q\rho\sqrt{q}\ell_m \tag{22}$$

and $C_q=0.09$. The corresponding values of k_T and D_T are found from Eqs. (19) and (20).

Chemistry

Chemistry representations can be classified as frozen, equilibrium, or finite rate. For combustion, the latter two can be further subdivided. For flow in a combustor with temperatures below about 2500 K for the H-C-O-N system, the flame sheet model [which limits the composition in the subregions of the flow to only fuel (H_2, CO) and products or to oxidant (O_2) and products] can provide good representations of equilibrium.[13] That approach, however, has no direct analog in the nozzle beyond the flame. The finite-rate models can be divided into "complete" (e.g., Ref. 3) or "global."[21] The considerations involved in making a choice of model are important, since cost is involved. For example, the formalisms involved in determining equilibrium compositions are well known and comprehensive, efficient, and easily usable codes such as Ref. 22 are available. However, even after restricting that code to the H-C-O-N system and removing many options unneeded for this work, the cost for an (h,p) entry on the APL IBM 3033 is on the order of 1¢. For perspective, a problem with a 20×30 space grid and 400 time steps could incur costs for equilibrium calculations alone of about $2000. That is sobering, especially when one recalls that local equilibrium is only an approximation to reality.

The choice of chemical model also can interact with the numerical solution of the fluid dynamics problem. If explicit methods are used, there are stability limitations on the step size. For cases where the characteristic fluid dynamics times are orders of magnitude different than the characteristic finite-rate chemical times, the selection of suitable step sizes for each can present problems. From an engineering viewpoint, however, this problem can be more apparent than real. If the chemical times are very small compared to flow times, the flow can be taken as in local equilibrium. If the chemical times are orders of magnitude larger than the flow times, one can assume premixing. If the chemical times are long compared to the flow transit time through a device (or component), it is appropriate to assume frozen flow.

To this point in our work for combustors and nozzles, we treat frozen flow, local equilibrium, a double flame sheet model,[13] and a simple global finite-rate scheme that uses a flame sheet model for

$$H_2+\tfrac{1}{2}O_2\rightarrow H_2O \tag{23}$$

with a rate equation for

$$CO+\tfrac{1}{2}O_2\rightarrow CO_2 \tag{24}$$

from Ref. 21. The last two schemes are really suitable only for combustor calculations.

For a hydrogen-fueled scramjet, one can assume, as a first approximation, that the hydrogen atom recombination reaction

$$H+H+M\rightarrow H_2+M \tag{25}$$

is the most important finite-rate process in the nozzle to the exclusion of the other possible reactions involving H-O-N. Note that the backward reaction is also neglected in this model.

Any problems created by very different flow and chemical times for explicit methods for the flow equations can be alleviated by treating the chemical production terms in an implicit manner,[23] and it happens that such an approach is very simple with the chemical model proposed above.

For some ranges of conditions, frozen flow in the nozzle is actually a good representation of reality. This is generally true when the concentrations of H and OH are low at the nozzle entrance. In any event, inexpensive estimates of the magnitude of the chemical effects to be expected for a given case can be made using a one-dimensional code such as described in Ref. 3.

Boundary and Initial Conditions

It was decided not to try to resolve the nozzle wall boundary layer within the full Navier-Stokes formulation. Instead, that is done separately using a TKE boundary-layer code that can accept rapidly varying edge boundary conditions such as produced by the mixing (and burning) in the core flow of the nozzle (and/or combustor). The "wall" boundary conditions for the Navier-Stokes, core flow calculation correspond to an insulated, impermeable surface with velocity slip. The solution values for the core flow evaluated at the "wall" serve as edge conditions for the boundary-layer calculation. In the language of perturbation methods, the Navier-Stokes core flow solution represents the "outer solution" (the same role as played by the inviscid solution in the usual boundary-layer theory) and the wall boundary-layer solution is the "inner solution." The compuational cost savings are substantial.

The "wall" formulation described above also impacts the inflow and outflow boundary conditions in a helpful way. Except for the wall boundary layer, the flow leaving the combustor and thus entering the nozzle is everywhere supersonic. Unless the nozzle is operating severely off-design, the same is surely true for the outflow. Thus, the inflow and outflow conditions for the Navier-Stokes core flow calculation are everywhere supersonic. This obviates the arguments over the best choices for inflow/outflow boundary conditions.[24] The inflow boundary conditions are determined from a combustor calculation such as in Ref. 13. The outflow boundary conditions are extrapolated.

Numerical Methods

The numerical method used for this work is the explicit, unsplit MacCormack scheme presented in Ref. 16. This finite-difference scheme is two-step, uncentered, and second-order accurate. Backward differences are used for the first step and forward differences are used for the second. This scheme was chosen because it is accurate and well tested. Also, explicit methods are enjoying a renewed popularity with the wider use of vectorized computations.

The computer code used was developed by modifying and extending the well-documented code of Cline.[17] He worked with the nonconservative form of the equations, which leads to shock smearing. However, strong shocks are rarely encountered in nozzles, so that was not deemed a serious limitation for the present application. That code was found to be carefully organized and clearly written, so that it was convenient to disassemble it, make substantive changes, add some things and delete others, and then reassemble everything into a workable package. Cline maps a general physical region into a rectangular computational region with a uniform grid spacing. This produces a grid arrangement in the physical space that has one set of straight grid lines in the y direction and curved grid lines that approximately follow the wall contour in the x direction. Nonuniform physical grid spacings may be specified. Cline also provided for subcycling and a "quick-solver" procedure for resolving boundary layers near solid surfaces, but those features were not needed here and were deleted. Cline's method has an artificial viscosity model to stabilize the shock wave calculations and provisions for time and/or space smoothing.

Since the MacCormack finite-difference scheme used is explicit, it is only conditionally stable and there is a time step size limitation,

$$\Delta t = \min(\Delta t_x, \Delta t_y) \tag{26}$$

where

$$\Delta t_x = \frac{A}{(|u|+a)/\Delta x + \mu_T/A_1\rho(\Delta x)^2}$$

$$\Delta t_y = \frac{A}{(|v|+a)/\Delta y + \mu_T/A_1\rho(\Delta y)^2} \tag{27}$$

The recommended values for the constants A and A_1 are 0.9 and 0.25, respectively. This restriction means that the time steps are limited such that sound waves travel less than one mesh spacing. For flows where the velocity is everywhere supersonic, this limitation results in a lesser number of time steps to reach steady state compared to cases with subsonic regions. This serves as a further justification of the present choices of numerical method for the core flow problem and also of calculating the wall boundary layer separately with a boundary-layer code.

The substantive extensions of the code of Ref. 17, which is limited to a single-specie, perfect gas with constant λ, that we found necessary for the scramjet nozzle core flow problem fell into five categories. First, it was necessary to add specie continuity equations to the system of equations for 10 molecular species: O_2, H_2, H_2O, N_2, CO, CO_2, H, OH, O, N. These equations are solved numerically, paralleling the methods used for the momentum equations. Second, the energy equation had to be extended to include additional terms for local changes in mixture molecular weight and for energy transfer due to mixing of species. The numerical solution of the extended energy equation was modified correspondingly. Third, the equation of state had to be extended for mixtures. Fourth, thermodynamic properties for the species of interest had to be included, i.e., c_{v_i}, e_i^0, etc. Finally, provisions for implementing the chemical model options (frozen, equilibrium, or global finite-rate) had to be included. Of course, the input and output also had to be modified to accommodate the additional flow variables.

Results

The main purpose here was to develop an analysis to predict the flowfield in a scramjet nozzle including the effects of strong nonuniformities in the inflow and turbulent mixing of those nonuniformities in the nozzle itself. To illustrate the capabilities of the method developed and the influence of these effects, a realistic, "generic" scramjet nozzle design case was selected. The case chosen is an example of an integral rocket/dual-combustion ramjet.[25] During the boost phase, the combustion chamber is filled with a solid propellant, incoming air ducts are blocked with frangible port covers, and the external compression surfaces are covered by a low-drag shroud. When the rocket propellant is consumed, the expendable rocket exit nozzles, frangible port covers, and the inlet shroud are ejected, air enters the inlet and the engine functions as a dual-combustion ramjet. The externally compressed air is subdivided by an inner cowl lip such that a fraction is ducted to a small, subsonic combustor. All of the fuel is added in the subsonic combustor, which acts as a fuel-rich, hot-gas generator for the supersonic combustor. The major portion of the air bypasses the gas generator and is ducted to the supersonic combustor, where it mixes and burns with the exhaust of the gas generator. The scramjet combustion chamber is axisymmetric with a central, coaxial fuel jet composed of a hot mixture of H_2, CO, H_2O, and N_2.

Detailed calculations have been made for a representative engine based on inlet design D from Ref. 25. Some of the features of this engine are:

1) The inlet compression surface is a 12.5 deg half-angle cone followed by an isentropic turn to a maximum surface angle of 27.1 deg.

2) Of the air captured by the inlet, 25% is ducted to the gas generator.

3) The design Mach number is 7 where the the critical pressure recovery is 0.10 in the gas generator.

4) At $M_0=4$, the inlet air capture ratio is 0.42 and the critical pressure recovery in the gas generator is 0.46.

5) The inlet to the main combustor internally contracts the flow by 16%, giving conditions ahead of the combustor shock of $M=2.23$ at $M_0=4$ and $M=3.53$ at $M_0=7$.

6) The ratios of gas generator area and main combustor inlet area to engine inlet area are 0.0458 and 0.0717, respectively.

7) The combustor is a cone frustrum with an exit-to-inlet area ratio of 3 and a length of 1.52 m.

8) The radius of the sonic exit of the gas generator is 6.5 cm and the blunt base has a thickness of 2.5 cm.

Combustor flowfield calculations for this case were given in Ref. 13 for flight conditions of Mach 7 at 18,500 m and Mach 4 at 11,400 m with Shelldyne H fuel at an overall equivalence ratio of 0.5. The results of those calculations at the end of the combustor can be used to give complete inflow conditions for the nozzle calculation.

Since the aim here is to show the effects of a nonuniform inflow on nozzle performance, nozzle designs developed assuming a uniform inflow were selected for study. The design contours were obtained by Van Wie at the Applied Physics Laboratory with his new nozzle design method,[26] which uses an inviscid flowfield analysis coupled to an optimization procedure to produce a design with the maximum thrust for a given nozzle length and area ratio. Nozzles were designed for the $M=7$ condition above with an "equivalent uniform" inflow determined to have the same static pressure and mass flow as the real nonuniform inflow, but assuming a composition of simply air with a Mach number of 2.10. The equality of the mass flow condition set the equivalent density. The actual nonuniform and the assumed "equivalent uniform" profiles are shown in Fig. 1. A nozzle length of 0.76 m and an exit radius of 24.1 cm was specified.

Two different nozzle designs were designed by Van Wie using his optimization procedure: one with an initial angle of 0 deg and the other with an initial, sharp-corner, 10 deg turn. A sharp turn of about this magnitude is good from the viewpoint of aerodynamics, but the attendant rapid expansion may produce chemical "freezing" in the nozzle. The two nozzle contours are shown in Fig. 2. The plots also show the Mach number contours predicted by Van Wie for the "equivalent uniform" inflow profiles and a constant γ of 1.4.

The Mach number profiles across the nozzle exit for the first nozzle design predicted by the present Navier-Stokes calculations for the real and "equivalent" uniform (all air but variable γ) inflows are shown in Fig. 3. These and all results presented here were made with frozen chemistry. This assumption is justified by the negligible amounts of O, H, and OH present at the combustor exit (nozzle inflow) for this particular case. Under those circumstances, "freezing" in the nozzle is not an important issue.[3] For other cases with higher static temperatures, the situation could be quite different and the frozen chemistry assumption would not be appropriate. Three results are plotted: the "equivalent" uniform inflow and two with the real inflow profiles. The latter two are for turbulence modeled with a mixing length and a TKE model. There is little difference between these two in Mach number. It is interesting that the exit Mach number profiles for the real, nonuniform inflow are somewhat more uniform than that for the "equivalent" uniform inflow.

A more meaningful display of the results is in terms of mass flux profiles as in Fig. 4, which shows profiles normalized with the outer edge (subscript e) value for each case. That value differs from case to case as indicated in Fig. 4. The values for the two real inflow cases is almost the same (difference less than 0.4%). Here, one can see that the real, nonuniform inflow results in a more nonuniform outflow. The calculations with the TKE model are slightly more uniform, since that model predicted more rapid mixing in the nozzle than the mixing length model. This is illustrated in Fig. 5 where O_2 concentration profiles at the exit are given. The TKE results are somewhat more mixed toward uniformity.

A nozzle calculation takes about 400 time steps to reach steady state, starting when a reasonable initial estimate of the flowfield (a simple one-dimensional calculation is made). That corresponds to a flow time roughly equal to three transits of the nozzle, front to back. The present calculations were made with a 33×21 grid, taking about 12 min of CPU time on an IBM 3033. To test the adequacy of the grid chosen, the calculation for the "equivalent" uniform all-air inflow case was compared to an inviscid calculation of Van Wie using a 150×50 grid with $\gamma=1.34$ to correspond to the high temperature "air." A comparison in terms of exit Mach number profiles is shown in Fig. 6 (note the expanded Mach number scale). The level of agreement shown can be taken as justification for the grid spacing used in our Navier-Stokes calculations. Also, the total mass flow at each axial station in the duct was checked; the largest deviations found were 0.4%.

The predictions for nozzle II are shown in Fig. 7 in terms of exit Mach number profiles. Again, the nonuniform, real inflow results in a slightly more uniform exit Mach number profile, even though this nozzle has a rapid initial expansion. The mass flux profiles at the exit plotted in Fig. 8 show,

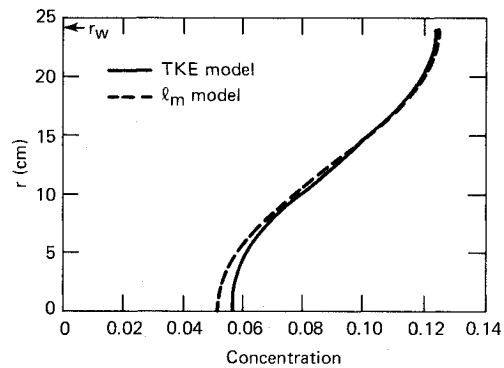

Fig. 5 Nozzle exit O_2 concentration profiles for nozzle I.

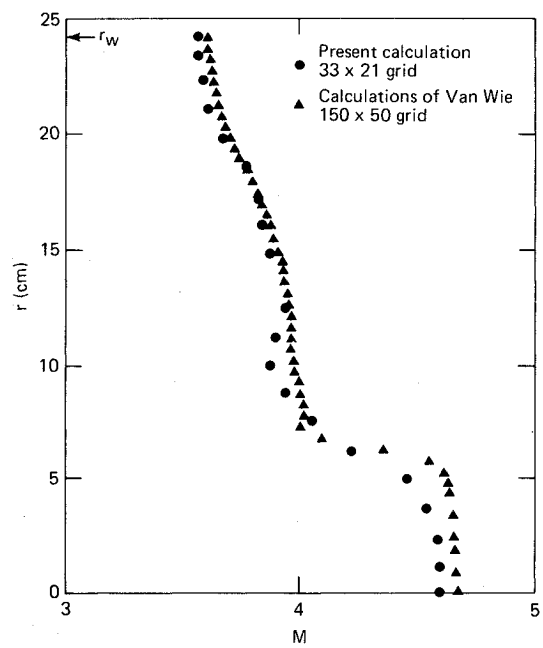

Fig. 6 Comparison of calculations with different grid spacing: exit Mach number profiles.

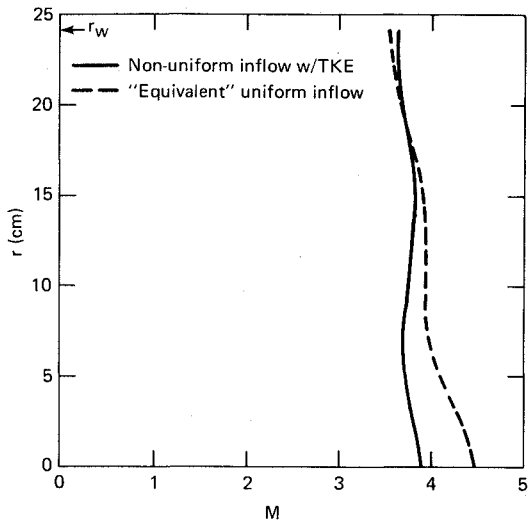

Fig. 7 Nozzle exit Mach number profiles for nozzle II.

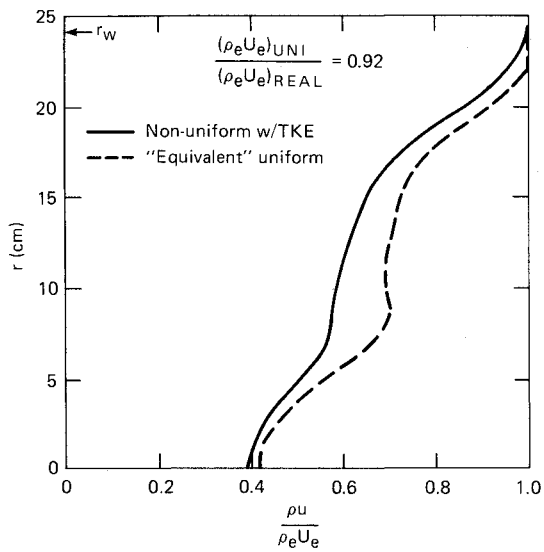

Fig. 8 Nozzle exit mass flux profiles for nozzle II.

however, that the nonuniform inlet profiles produce more nonuniform exit profiles than the uniform inflow case. Comparing Figs. 4 and 8, one can say that the more rapid initial expansion design (nozzle II) produces somewhat more nonuniform exit profiles. This is based on examining the profiles at the larger radii where most of the mass flow passes because of the axisymmetric geometry.

Wall boundary-layer calculations were run for the scramjet with nozzle II and the skin-friction results are shown in Fig. 9 where $C_f = \tau_w / \frac{1}{2}\rho_e U_e^2$. The skin-friction coefficient falls with distance in the inlet duct, shows a bump in the simulated precombustion pressure rise region, rises, then remains roughly constant in the combustor, pops up again at the beginning of the nozzle due to the rapid initial expansion, and then falls. The C_f values do not look very different from the end of the combustor to the end of the nozzle, but the actual wall shear τ_w values have fallen to only about 25% of the combustor exit value by the end of the nozzle. One might like to begin the expansion process sooner to decrease the surface area with high wall shear. At the nozzle entrance, the duct radius is almost 10 cm and the boundary-layer momentum thickness is 0.30 cm. At the nozzle exit, the duct radius is about 24 cm and the momentum thickness has grown to 0.70 cm. It is also useful to estimate the total heat and momentum transfer through the boundary layer to the

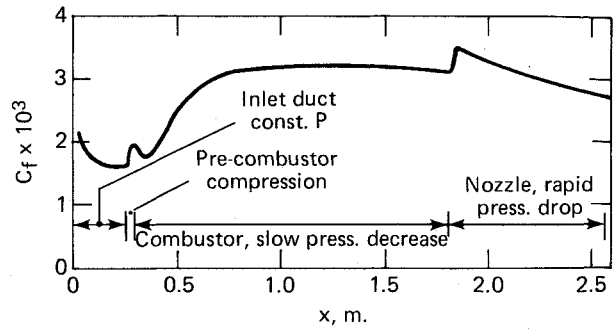

Fig. 9 Skin-friction distribution for scramjet with nozzle II.

wall, since those losses have been neglected in the core flow calculation. For this case, the heat loss compared to the energy in the stream and the momentum loss by drag compared to the stream momentum were each less than 2%.

The boundary-layer calculation along the whole length took about 1 min of CPU time on an IBM 3033, so the nozzle portion took about 0.5 min. Thus, splitting the nozzle core flow and wall boundary-layer calculations resulted in a total CPU time of about 12–13 min.

Discussion

A complete procedure for calculating the flowfield and performance of scramjet nozzles has been developed. To minimize computer cost, the nozzle core flow and the nozzle wall boundary layer are treated separately. A major difference between the current procedure and earlier nozzle calculations is that the core flow is now treated as a fully viscous, turbulent region with mixing and chemical reactions using the Navier-Stokes equations. The separate treatment of the wall boundary layer permits good resolution of the flow in that region and accurate skin-friction and heat-transfer predictions. Finally, this new procedure can accept essentially arbitrary, nonuniform nozzle inflow profiles.

The calculations presented are for a vehicle designed as an assembly of separate components. Thus, the combustor was purposefully made rather long to minimize the nonuniform profile effects on nozzle performance. With the new computational capacity demonstrated here, it is now possible to design efficient nozzles to operate with strongly nonuniform inflow profiles. This will permit shorter combustors and shorter, lighter vehicles.

Acknowledgment

This work was supported by the U.S. Naval Ordnance Systems Command.

References

[1]Waltrup, P. J., Billig, F. S., and Stockbridge, R., "A Procedure for Optimizing the Design of Scramjet Engines," *Journal of Spacecraft and Rockets*, Vol. 16, May-June 1979, pp. 163-172.

[2]Weber, R. J. and MacKay, J. S., "An Analysis of Ramjet Engines Using Supersonic Combustion," NACA TN 4386, Sept. 1958.

[3]Westenberg, A. A. and Favin, S., "Complex Chemical Kinetics in Supersonic Nozzle Flow," *Ninth Symposium (International) on Combustion*, Academic Press, New York, 1963, pp. 785-797.

[4]Lezberg, E. A. and Lancashire, R. B., "Recombination of Hydrogen-Air Combustion Products in an Exhaust Nozzle," NASA TN D-1052, 1961.

[5]Franciscus, L. C. and Lezberg, E. A., "Effects of Exhaust Nozzle Recombination on Hypersonic Ramjet Performance, II: Analytical Investigation," *AIAA Journal*, Vol. 1, Sept. 1963, pp. 2077-2083.

[6]Ferri, A., "Review of Scramjet Propulsion Technology," *Journal of Aircraft*, Vol. 5, Jan. 1968, pp. 3-10.

[7]Migdal, D., Hammer, S., and Agosta, V., "Scramjet Combustor and Nozzles Analysis for Two Phase Flow," Propulsion Sciences Inc., Melville, NY, Rept. 68-1, Jan. 1968.

[8]Agosta, V. and Hammer, S., "Scramjet Nozzle Analysis," Propulsion Sciences Inc., Melville, NY, Rept. 70-1, Feb. 1970.

[9]"Hypersonic Research Engine Project Technological Status 1971," NASA TM X-2572, Sept. 1972.

[10]Waltrup, P. J., Anderson, G. Y., and Stull, F. D., "Supersonic Combustion Ramjet (SCRAMJET) Engine Development in the United States," Paper 76-042 presented at 3rd International Symposium of Air Breathing Engines, Applied Physics Laboratory, Johns Hopkins University, Laurel, MD, 1976.

[11]Ferri, A., Libby, P. A., and Zakkay, V., "Theoretical and Experimental Investigation of Supersonic Combustion," *Proceedings of International Council on Aeronautical Sciences, 1962,* Macmillan, London, 1964, pp. 1089-1155.

[12]Drummond, J. P., Rogers, R. C., and Evans, J. S., "Combustor Modelling for Scramjet Engines," AGARD CP-275, Oct. 1979, Paper 10.

[13]Schetz, J. A., Billig, F. S., and Favin, S., "Flowfield Analysis of a Scramjet Combustor with a Coaxial Fuel Jet," *AIAA Journal,* Vol. 20, Sept. 1982, pp. 1268-1274.

[14]Drummond, J. P. and Weidner, E. H., "Numerical Study of a Scramjet Engine Flowfield," *AIAA Journal,* Vol. 20, Sept. 1982, pp. 1182-1190.

[15]Dash, S. M. and Wolf, D. E., "Fully-Coupled Analysis of Jet Mixing Problems," NASA CR 3761, Jan. 1984.

[16]MacCormack, R. W., "The Effect of Viscosity in Hypervelocity Impact Cratering," AIAA Paper 69-354, April 1969.

[17]Cline, M. C., "VNAP2: A Computer Program for Computation of Two-Dimensional, Time-Dependent, Compressible, Turbulent Flow," Los Alamos National Laboratory, Los Alamos, NM, Rept. LA-8872, Aug. 1981.

[18]Aris, R., *Vectors, Tensors and the Basic Equations of Fluid Mechanics,* Prentice-Hall, Englewood Cliffs, NJ, 1962.

[19]Schetz, J. A., *Foundations of Boundary Layer Theory,* Prentice-Hall, Englewood Cliffs, NJ, 1984.

[20]Schetz, J. A. (ed.), *AIAA Progress in Astronautics and Aeronautics: Injection and Mixing in Turbulent Flow,* Vol. 68, AIAA, New York, 1980.

[21]Westbrook, C. K. and Dryer, F. L., "Simplified Reaction Mechanisms for the Oxidation of Hydrocarbon Fuels in Flames," *Combustion Science and Technology,* Vol. 21, 1981, pp. 31-43.

[22]Svehla, R. A. and McBride, B. J., "FORTRAN IV Computer Program for Calculation of Thermodynamic and Transport Properties of Complex Chemical Systems," NASA TN D-7056, Jan. 1973.

[23]Smoot, L. D., Hecker, W. C., and Williams, G. A., "Prediction of Propagating Methane-Air Flames," *Combustion and Flame,* Vol. 26, 1976, pp. 323-342.

[24]Oliger, J. and Sundström, "Theoretical and Practical Aspects of Some Initial Boundary Value Problems in Fluid Dynamics," *SIAM Journal on Applied Mathematics,* Vol. 35, 1978, pp. 419-446.

[25]Billig, F. S., Waltrup, P. J., and Stockbridge, R. D., "The Integral-Rocket, Dual-Combustion Ramjet: A New Propulsion Concept," *Proceedings of 4th International Symposium on Air Breathing Engines,* AIAA, New York, April 1979, pp. 433-444.

[26]Van Wie, D., "An Application of Computational Fluid Dynamics to the Design of Optimum Ramjet Powered Missile Components," Ph.D. Thesis, University of Maryland, College Park, 1986.